Multiscale modeling of precipitation hardening: application to the Fe-Cr alloys

Ghiath Monnet

EDF – R&D, MMC, avenue des Renardières, 77818 Moret sur Loing, France. Email: ghiath.monnet@edf.fr

Abstract

Precipitation Hardening is investigated using Dislocation Dynamics (DD) simulations. Unlike classical approaches, precipitates are represented by an interaction potential, completely determined from Atomistic Simulations (ASs), including size and temperature effects. The transition method is first validated by comparing DD and ASs of interactions with one precipitate using the same simulation conditions and, then, applied in massive DD simulations for the prediction of hardening as a function of precipitate size, density and shear resistance over a large range of temperature. Results show that hardening is always proportional to the Orowan hardening with an interaction coefficient depending on the effective resistance of the precipitates. A simple theoretical model is found to describe appropriately the ensemble of the reported results.

1. Introduction

Precipitation Hardening (PH) is one of the oldest features used to improve the mechanical properties of alloys [1,2]. Although it has been discovered one century ago, its precise determination is still delicate. It is often superposed to other hardening sources such as forest [3] or solid solution hardening [4]. On the theoretical level, many assumptions and simplifications must be considered in order to reduce the large number of degrees of freedom associated to the interaction between mobile dislocations and the precipitate population: precipitate size, distribution and density, the interaction range and potential, testing temperature and strain rate, etc. [5,6].

With the notable increase in computational capabilities in terms of memory storage, access and clock speed, numerical simulations provided deep insights into the hardening mechanisms induced by precipitation. Foreman et al. [7] were the first to use numerical simulations to study the role of precipitate distribution and strength, while Bacon et al. [8] were the first to reveal by quasi-static DD simulations the effect of precipitate size on hardening in the case of the Orowan mechanism. They also proposed a pioneering model (called BKS model in the following) accounting for the effect of the random distribution.

However, for coherent and shearable precipitates, both theory and numerical simulations encounter the same fundamental difficulty: the construction of the interaction potential with dislocations, which controls not only the precipitate strength [5] but also the interaction statistics [7,9], the temperature and strain rate effects [10]. Many potentials were reported in the literature [5] depending on the interaction mechanisms, such as modulus [11], lattice [12] and stacking fault [13] mismatches. However, the approximations used are systematically

strong, such as the straight-line approximation. Besides, more than one mechanism are usually involved in the interaction, making the prediction of the global interaction potential a difficult task.
In this context, Atomistic Simulations (ASs) constitute a powerful tool to identify the interaction nature and potential [14]. In most cases, ASs confirm that the unpinning stress varies with temperature, dislocation character and precipitate nature (e.g. shearable vs non-shearable) and size. But the identification of the interaction potentials from AS results is still not straightforward. Some methods were proposed to compute the activation energy as a function of the applied stress from ASs of dislocation nucleation [15,16] and motion in high Peierls-barrier dislocations [17,18]. However, these methods cannot be applied in the case of local obstacles. Dislocation curvature induces stress concentration on the pinned segments, which may exceed significantly the applied stress. Monnet [19] and Khater et al. [20] have shown that the appropriate state variable of the activation energy is the effective stress, i.e. the local stress on the segments in contact with the precipitate.
Even when the interaction potential is identified using ASs, larger scale simulations are required to predict dislocation interaction with a large number of precipitates. In the first reported studies, precipitate strength was introduced as a critical cusp angle using the constant line tension approximation [21,22] including thermal activation [23,24]. But this method does not account for dislocation-dislocation interactions and neglects the precipitate size effects. These flaws can be overcome using the DD simulation technique, where precipitates of finite size of arbitrary distribution can be mapped into the simulation box and dislocation-dislocation interactions are fully accounted for. The first DD investigations of PH were reported by Flush et al. [25] and Mohles et al. [26] and extended later to different interaction mechanisms [27,28]. Although a thorough progress has been made in these studies, the interaction potential was not built using ASs.
The objective of this paper is to present the first full multiscale simulations of precipitation hardening. ASs are used to determine the interaction potential and the associated activation energy. Then DD simulations are used to compute PH within a large range of precipitate strength, size, density and simulation temperature and strain rate. The results obtained are used to develop a simple theoretical model of PH without adjustable parameter. The case of Cr precipitates in iron is considered as illustrative example of the multiscale approach.
The paper is organized as follows. First, the transition method is presented and validated using the illustrative example. Then, DD simulations of PH as a function of the precipitate resistance, size, testing temperature and strain rate are reported. In the last section, we discuss the results obtained in connection with theoretical model and present the analytical model of precipitate hardening.

2. The multiscale simulation approach

2.1. From atomistic simulations to dislocation dynamics

The full details of the transition method used here were reported in [29]. Here we recall the basic concepts. As widely known in DD simulations, the stress computed in the center of a segment or on adjacent nodes (the effective stress) fully controls its behavior. The main idea of this transition method is to interpret the AS results as a function of the effective stress on the dislocation segment pinned by the precipitate. This approach has already been used in analytical approaches [5] and in DD simulations of precipitate hardening [30,31]. At zero K, a given precipitate cannot keep a dislocation segment pinned when it is submitted to an

effective stress τ_{eff} larger than a critical value, called the obstacle resistance τ_{obs}. For example, if the shearing process creates an antiphase surface, τ_{obs} is equal to γ/b [30], where γ is the antiphase surface energy and b the norm of the Burgers vector. τ_{obs} is naturally connected to the classical strength F_{obs} by $F_{obs} = Db\tau_{obs}$, where D is the diameter of the precipitate, considered to be of spherical form in all AS and DD simulations. From ASs at 0 K, it is easy to compute the resistance stress using the equation:

$$\tau_{obs} = \frac{l}{D}(\tau_{max} - \tau_f), \qquad (1)$$

where l stands for the free distance between precipitates, i.e. the distance between the precipitate centers L minus D, τ_{max} the maximum applied stress (unpinnging stress) recorded in ASs and τ_f is the friction stress for dislocation motion in the matrix. Of course, Eq. (1) holds when the dislocation slip plane passes by the precipitate center. Otherwise, D must be replaced by the effective diameter of the interaction circle. In the review reported in [29], τ_{obs} was computed for voids and Cu precipitates in iron using ASs [32,33]. In Fig. 1, these data are reproduced together with the resistance of Cr precipitates τ_{Cr} for comparison. ASs used to compute τ_{Cr} have been reported by Terenteyev et al. [34,35]. Four important remarks can be already made: (i) for sufficiently large defects (say larger than 1.5 nm), the resistance stress τ_{obs} is independent of the defect size; (ii) the resistance of voids (4.8 GPa) is much larger than those of Cu (2.4 GPa) and Cr precipitates (2.1 GPa); (iii) small defects (less than 1.5 nm) systematically offer less resistance than large ones and (iv) the obstacle resistance is independent of the dislocation length. These features confirm that τ_{obs} is an intrinsic characteristic of the precipitate nature. According to Eq. 1, if the resistance stress is constant, defect strength F_{obs} becomes proportional to the defect size.

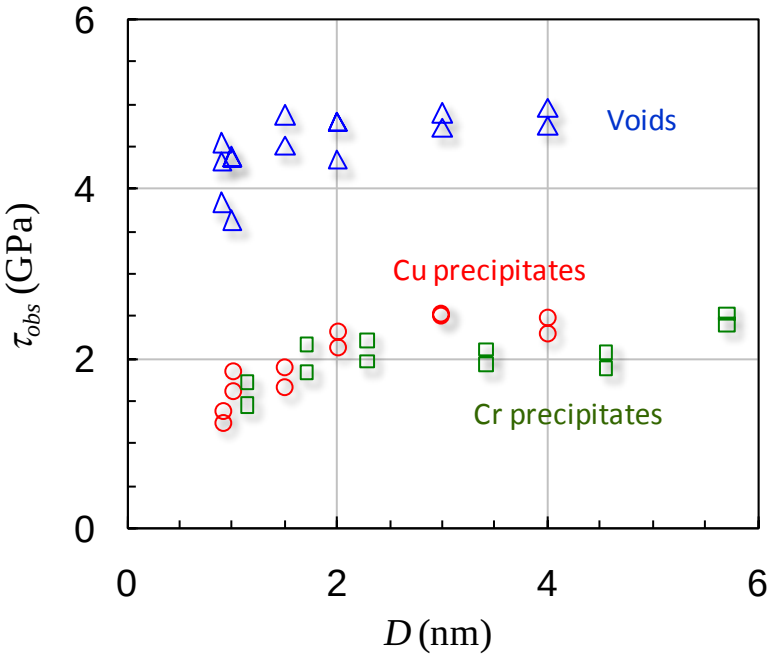

Fig. 1: resistance of different defect types in iron as a function of the defect size: voids (triangles), Cu precipitates (circles) and Cr precipitates (rectangles), computed from atomistic simulations with different dislocation lengths.

In the rest of the paper, τ_{obs} will be a variable representing the defect resistance. The case of Cr precipitates will be considered as case study for specific applications. These precipitates appear after neutron irradiation of FeCr ferritic alloys [36,37], which are of technological importance in future nuclear reactors [38].

2.2. Determination of the activation energy

MD simulations reveal a temperature effect on the unpinning stress of Cr precipitates [34,35]. The determination of the corresponding activation energy ΔG allows accounting for thermal activation at larger scale simulations, such as DD simulations [39] and constant line tension simulations [40]. In all cases, the determination of ΔG from ASs requires a stochastic analysis of MD results [17,18]. The details of the analysis method used in this work were published in [19]. Here we recall the basic features. First we compute from ASs the effective stress on the pinned segment during loading. Then, the evolution of the effective stress is used to determine the Poisson's stress, i.e. the constant effective stress that would provide the same activation probability at the end of the pinning time. This stress regularization is necessary to model the unpinning rate by a Poisson's process, which is implicitly assumed in the Arrhenius-type activation rate [41]. Last, ΔG is computed as a function of the Poisson's stress. The analysis results are depicted in Fig. 2a. The largest value of ΔG computed within MD simulations was 0.71 eV. ΔG decreases and tends as expected to zero when the Poisson's stress approaches the Cr-precipitate resistance τ_{Cr}. When τ_{eff} is larger than τ_{obs}, the Cr-precipitate is of course sheared athermally and instantaneously.

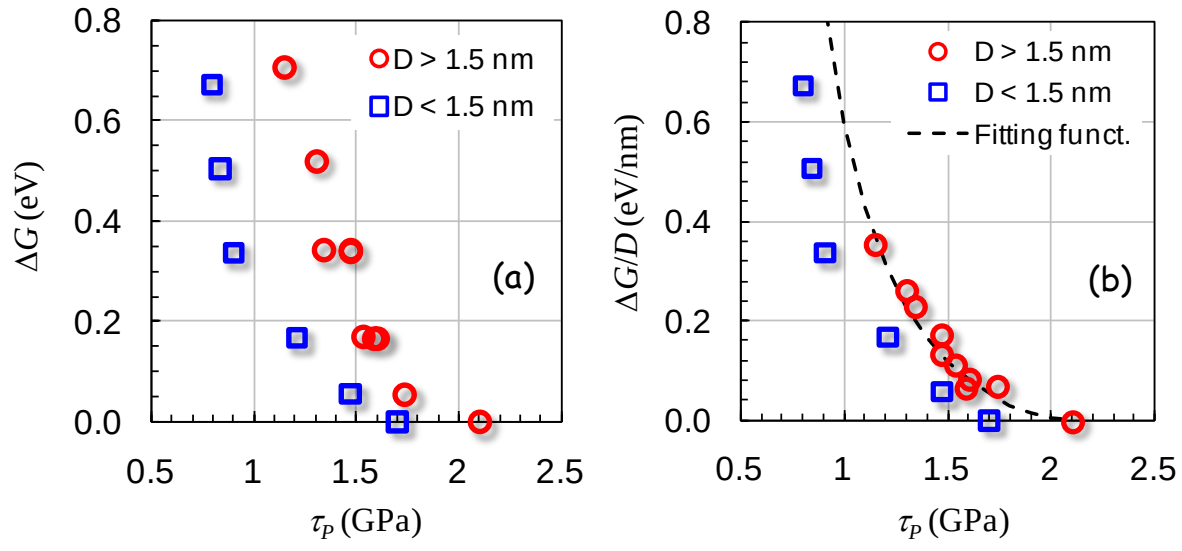

Fig. 2: (a) evolution of the activation energy and (b) the activation energy normalized by the precipitate size as a function of the Poisson's stress for Cr-precipitates of different size and dislocation lengths. The dashed line is the numerical fit on data for D > 1.5 nm (Eq. 2).

A large dispersion can be noticed in Fig. 2a. Two reasons can be advanced for this. For $D <$ 1.5 nm, Cr-precipitates offer weaker resistance than other precipitates (see Fig. 1). On the

other hand, the activation energy is expected to vary with the precipitate sizes. The last feature can be understood since the activation energy is a function of the absolute force F of the precipitate, which is proportional to the precipitate size, since $F = Db\tau_{eff}$. Consequently, ΔG normalized by D is likely to be the appropriate function of the effective stress. In Fig. 2b, ΔG is normalized by D and data for the 1 nm precipitate are plotted using different symbol. Again, the 1 nm precipitate appears weaker than other precipitates for all the simulated temperatures. However, for the other precipitates, values of $\Delta G/D$ obtained in all ASs (different precipitate size, dislocation length and simulation box dimensions) are aligned on one single and smooth curve, indicating that the activation energy (like the precipitate strength) scales with the precipitate size. The following equation offers a good fit to MD simulation results for Cr precipitates of size larger than 1.5 nm :

$$\Delta G / D \text{ (in eV/nm)} = 0.3\left[\ln\frac{\tau_{Cr}-\tau_{ath}}{\tau_{eff}-\tau_{ath}}\right]^{1.6}. \qquad (2)$$

The curve representing Eq. 2 is plotted in Fig. 2b as a dashed line. Eq. 2 ensures that ΔG goes to zero when τ_{eff} goes to τ_{Cr} and goes to infinity when τ_{eff} approaches τ_{ath} = 0.7 GPa. The latter is a threshold value of the effective stress at which the activation energy and volume go to infinity. It represents the athermal part of the obstacle resistance that cannot be overcome by thermal activation. In other terms, the dislocation is kept pinned for infinite time as long as the effective stress on the pinned segments is less than τ_{ath}. The rate of the unpinning process is thus given by:

$$w = w_o \exp -\frac{\Delta G(\tau_{eff})}{kT}, \qquad (3)$$

where w_o is a frequency factor in the order of 10^{13} s^{-1} [19], k the Boltzmann constant and T the absolute temperature. The frequency factor is likely to be dependent on the dislocation length and/or the precipitate size. However, this dependency is of minor importance compared to the exponential dependency on the effective stress. It is thus neglected here. For an individual unpinning event, w represents the density of probability of activation. For large number of pinning precipitates, w corresponds to the number of activated precipitates per unit time, in agreement the definition of the Poisson's process.

2.3. Dislocations dynamics simulations

The description of the DD calculation method can be found in a separate paper [42]. We describe here only features peculiar to the present simulations. The DD simulation box is a rectangular parallelepiped, used to model a small BCC crystal, containing one or large number of randomly distributed precipitates. The x, y and z axes are parallel to the Burgers vector (½ [111]), to the normal of the slip plane ([$1\bar{1}0$]) and to the [$\bar{1}\bar{1}2$] direction corresponding to the direction of the edge dislocation line. At high enough temperature, the behavior of dislocations of different characters is considered to be similar [43]. This is why only edge dislocations are simulated in this study. In all DD simulations, periodic boundary conditions were applied in the three directions, resulting in an infinite edge dislocation.

A dislocation segment is allowed to move when the effective stress τ_{eff} computed at its center is larger than a threshold stress, called the friction stress τ_f. Its velocity is given by $v = b(\tau_{eff} - \tau_f)/B$, where B is the friction coefficient. In our simulations, we considered the values b = 0.25 nm and $B = 10^{-4}$ Pa.s for all dislocation characters. When a segment is found to

touch or inside the precipitate, its mobility follows another rule. At 0 K, τ_f is replaced simply by τ_{obs}, while at finite temperature the probability of motion is set according to the binomial distribution, known to tend to the Poisson's distribution for large iteration steps [29]. To reproduce the elastic behavior we consider the effective isotropic moduli proposed in [44,45] and provided for iron in [46]: a Poisson's ratio of 0.48 and a shear modulus μ of 63 GPa. The friction stress is taken equal to 80 MPa at 0 K and zero at finite temperature Different strain rates were simulated resulting in different dislocation velocities: 0.2, 2 and 20 m/s. These values are within the order of magnitude of dislocation velocity observed in classical mechanical tests of metals at enough high temperature [47].
The performed DD simulations can be separated into two categories. The "1-precipitate" simulations are dedicated to the validation of the scale transition method, with the simulation box dimensions and face orientations being the same as those used in ASs [34,35]. The "massive" simulations are used to compute PH induced by a large number of randomly distributed precipitates. The dimension perpendicular to the slip plane was reduced to 4 times the size of the precipitates. The other two dimensions were selected such that the dislocation length was larger than twenty times the average planner spacing and the simulation box contained approximately 20,000 precipitates. These precautions allow minimizing the size effects on the PH, reported by Nogaret et a. [21].

2.4. Validation of the transition method

When the obstacle strength is infinite, i.e. of Orowan type, the precipitate is bypassed. DD simulations of interaction with periodic row of precipitates [31,48] confirm predictions of Bacon-Kocks-Scattergood (BKS) model [8]. Precipitate of finite strength must induce lower hardening depending on the value of the obstacle resistance. In order to validate the transition method used here, 1-precipitate simulations of dislocation interaction with a Cr precipitate in iron were carried out in the same conditions as the atomistic simulations. Stress-strain curves of interaction with Cr precipitates of different sizes are plotted in Fig. 3a.

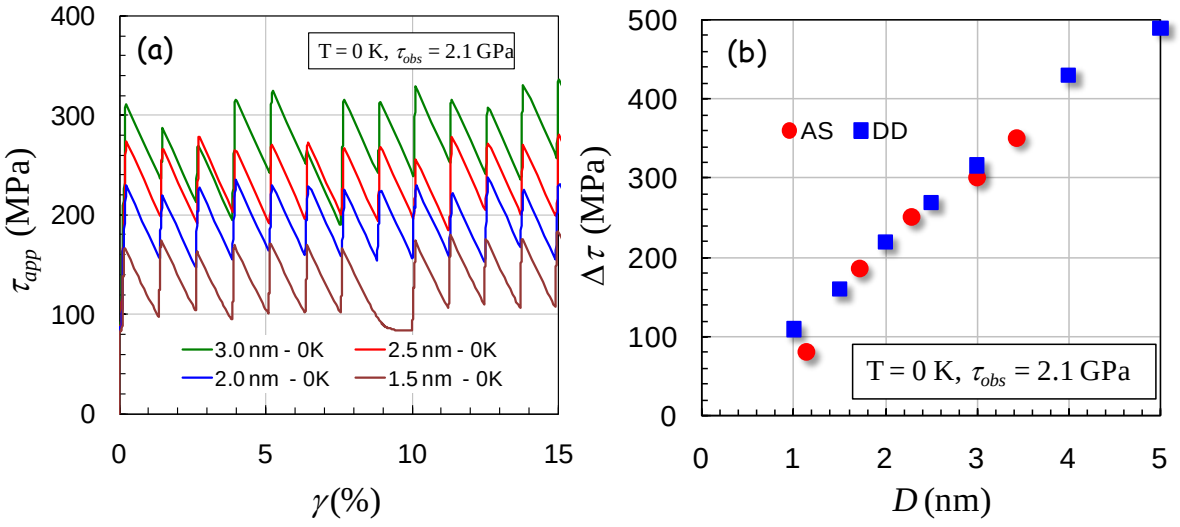

Fig. 3: (a) stress-strain curves of an edge dislocation of 21 nm length interacting with periodic row of Cr precipitates of different sizes and (b) comparison between the unpinning stress computed in DD and in ASs for different Cr-precipitate sizes at 0 K.

Thanks to periodic boundaries, the edge dislocation can interact several times with the precipitate, which allows for testing the reproducibility of the interaction strength. As it can be noticed on each curve, the stress maxima are close but not the same. For every interaction, the segment configuration in contact with the precipitate was found to be different, leading to a stochastic-type behavior. Since we are interested in interaction with a large number of precipitates, only the average of all maxima is pertinent. In all what follows, the average of stress maxima of the stress-strain curves will be considered as representative of flow stress in the presence of precipitates. The corresponding PH is obtained by subtracting the friction stress: $\Delta\tau = \tau_c - \tau_f$.

In Fig. 3b, DD results are compared with the ASs for different Cr-precipitate sizes, of resistance τ_{Cr} = 2.1 GPa. It can be seen that DD simulations correctly reproduce the pinning strength of the different precipitates. However, for the 1nm Cr-precipitate, DD prediction is larger than that provided by ASs, which reflects the fact 2.1 GPa, is not the appropriate the resistance of very small Cr-precipitates (see Fig. 1).

In a second step, we investigate the effect of the resistance τ_{obs} of a 2 nm precipitate on the unpinning stress (see Fig. 4a). $\Delta\tau$ is found to vary linearly with τ_{obs} for small τ_{obs} values, with a slope of 0.1, which is quite close to the slope expected from Eq. 2 and equals D/l = 0.11. For large values of τ_{obs} (say more than 3.5 GPa), $\Delta\tau$ reaches a saturation plateau. At the beginning of the plateau, the dislocation is found to shear the precipitate, while it bypasses it for τ_{obs} larger than 4.5 GPa. Surprisingly, the saturation of the unpinning stress does not correspond to the onset of precipitate bypassing. This feature is discussed later in the paper.

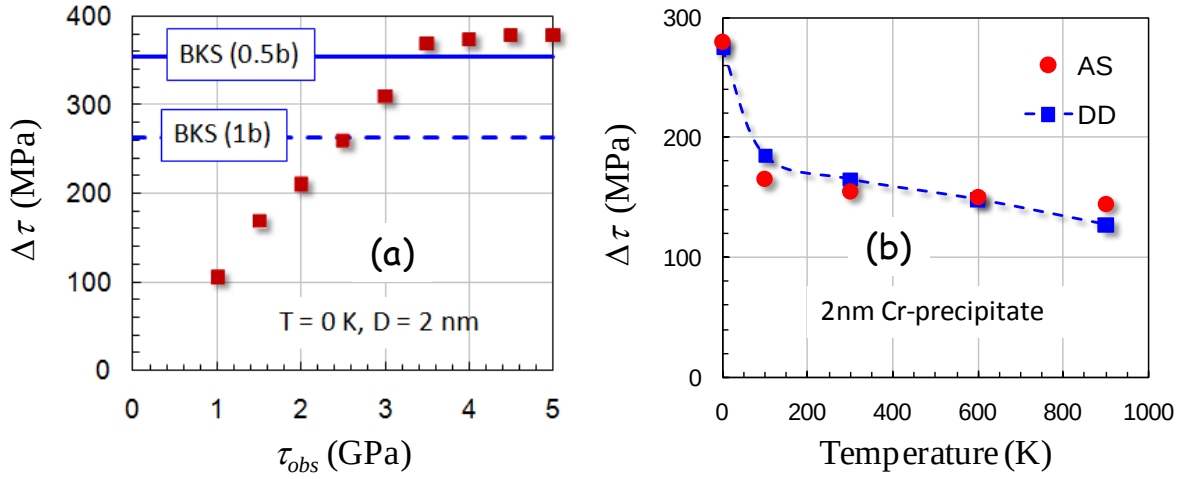

Fig. 4: (a) effect of the obstacle resistance of a precipitate of 2 nm on the unpinning stress computed in DD for a dislocation of 21 nm length. Predictions of the BKS model are shown with two normalization conditions; (b) comparison between the unpinning stress predicted by DD and ASs as a function of temperature for a 2nm Cr-precipitate.

The saturation stress (close to 380 MPa) is compared with the theoretical predictions of the BKS model of hardening induced by a periodic row of precipitates of size D and spacing l: $\Delta\tau_{BKS} = \mu b/(2\pi l) \ln \underline{D}$, where $\underline{D}$ is the harmonic mean of D and l: $\underline{D}=Dl/(D+l)$ normalized by the norm of the Burgers vector b. The prediction is shown in dashed line in Fig. 4a. It

amounts to 261 MPa, which is in poor agreement with the DD results. To improve the agreement, we consider the normalization by 0.5*b* instead of 1*b* (see § discussion for more details). The modified BKS model for the periodic row is:

$$\Delta\tau_{BKS} = \frac{\mu}{2\pi l}\ln 2\underline{D}\,, \qquad (4)$$

where all lengths were normalized by the length of the Burgers vector. The prediction of Eq. 4 is plotted as solid line in Fig. 4a and amounts to 355 MPa, which fits much better our DD simulation results.

The next validation step is to check the validity of the thermal activation parameters deduced from ASs and used in DD. The time integration method proposed in [29] for the activation rate given in Eq. 3 is applied here. DD simulations of 21-nm dislocation interacting with a 2 nm Cr- precipitate are conducted at different temperatures. The comparison between $\Delta\tau$ obtained in DD and in AS is shown in Fig. 4b. The friction stress introduced in Eq. 2 was fitted on AS for edge dislocation moving freely in iron [49]. We can notice from Fig. 4b that the temperature sensitivity of the interaction is similar to that revealed in ASSs. Notwithstanding, DD predictions seems to overestimate the temperature sensitivity. This is because of the smooth curve used to fit the activation energy profile in Fig. 2b.

3. Simulation Results

4. The Orowan hardening

When the obstacle strength is infinite, i.e. of Orowan type, DD results of hardening induced by periodic row [31] and randomly distributed obstacles [3,50] were found in agreement with the BKS model [8]. This agreement was obtained for large obstacles ($D >> b$) and when the average precipitate planner spacing l is much larger than the precipitate size diameter D. It is necessary thus to check the agreement with the BKS model for randomly distributed Orowan precipitates of nanometric size and large densities. To do so, massive DD simulations of Orowan hardening are conducted for obstacles of 1 and 2 nm size and of density varying between 10^{23} to 8×10^{24} m^{-3}. Following the disperse barrier hardening model [51], the average planner spacing L of precipitates of average size D and number density C is $(DC)^{-½}$, to be distinguished from the free spacing between the precipitates $l = L - D$, which is the appropriate length to consider in theoretical models and treatments. The first remark that can be made on the results depicted in Fig. 5 is that the size effect on the Orowan hardening is quite important for small particles. Passing form 1 to 2 nm in diameter, hardening is more than doubled, while the corresponding decrease in l amounts only to 40%.

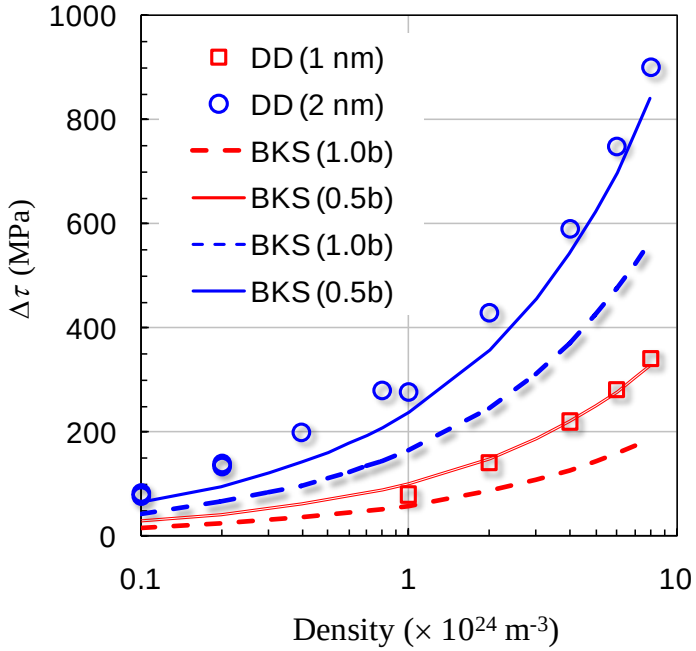

Fig. 5: DD prediction of the Orowan hardening compared with theoretical predictions of the BKS model, using two different normalization conditions.

DD results are then compared to the BKS model predicting Orowan hardening. Again, predictions of the initial BKS model, shown in dashed lines on Fig. 5, significantly underestimate the Orowan hardening revealed by DD simulations. The normalizing by 0.5*b* instead of *b* improves greatly the model predictions as can be shown in Fig. 5, where results of the new normalization are plotted in solid lines. The modified BKS model can thus be expressed as:

$$\Delta\tau_{BKS} = \left(\frac{\ln 2D}{\ln 2l}\right)^{3/2} \frac{\mu}{2\pi l}\ln(2l)\,, \qquad (5)$$

In Eq. 5, all lengths are normalized by the norm of the Burgers vector. The new normalization procedure is discussed later in the paper.

4.1. Hardening induced by precipitates of finite strength

In this section we investigate the effect of the precipitate resistance on PH computed in DD simulations without thermal activation. In a first step, we compare PH induced by the precipitates of finite resistance with that induced by the same population of precipitates of infinite resistance. To do so, we considered precipitates of different size (1, 2, 4 nm) and density ($1 - 8\times10^{24}$ m^{-3}) interacting with an edge dislocation at 0 K. For every configuration, two massive simulations were conducted: one with a resistance $\tau_{obs} = \tau_{Cr} = 2.1$ GPa and one with a resistance $\tau_{obs} = \infty$, which prevents any segment from penetrating the precipitate. The PH induced by the Cr precipitates is then plotted as a function of the Orowan hardening, as shown in Fig. 6a.

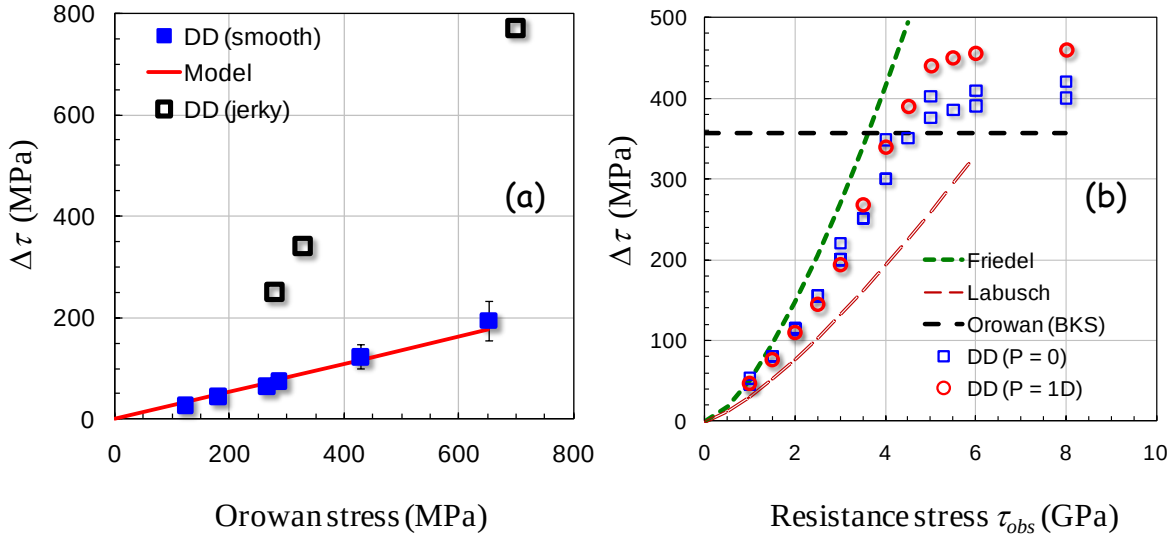

Fig. 6: (a) hardening induced by Cr precipitates as a function of the Orowan hardening, (b) precipitation hardening induced by 2 nm precipitates of 2×10^{24} m^{-3} density as a function of their resistance. Squares represent simulation of fully random distribution and circles simulations of a random distribution avoiding precipitate overlap. The Friedel and Labusch model predictions are depicted using dashed lines for comparison.

Two different modes of dislocation motion are observed in DD simulations, in agreement with other investigations [52]. In simulations with 1 nm (1×10^{24}, 2×10^{24} m^{-3}, 4×10^{24} m^{-3}) and 2 nm (1×10^{24} m^{-3}; 2×10^{24} m^{-3}; 4×10^{24} m^{-3}), the dislocation unpins successively from individual precipitate (the smooth mode). In the other configurations, the dislocation motion was jerky (jerky mode), where the dislocation unpins from a group of precipitates upon each unpinning event. It is easy to notice that in the smooth mode, hardening induced by Cr precipitates is significantly lower but remains proportional to the Orowan hardening. This confirms that interaction statistics in the smooth mode are the same for shearable and impenetrable obstacles. The difference in hardening results only from the obstacle strength. This remark does naturally not apply in the jerky mode.

In the next step, we investigate the sensitivity of the PH to the precipitate resistance. τ_{obs} is varied in massive DD simulations of interaction with precipitates of D = 2 nm and C = 2×10^{24} m^{-3}. Different distributions were tested in these simulations. First fully random distributions were generated for each value of τ_{obs}. In this distribution, the minimum distance between precipitate centers is zero. In Fig. 6b this distribution is referred to by P = 0 (P for Percolation). Moreover, since real precipitates do not intersect thanks to Ostwald ripening [53] (cited by [5]), additional random distributions are generated, where randomness is restricted by preventing precipitate overlapping. The minimum spacing between particle centers is the diameter of the precipitates D. These simulations are referred to as $P = D$ in Fig. 6b. Examination of the results confirm that PH increases with the obstacle resistance up to almost τ_{obs} = 4.5 GPa. Beyond this resistance, hardening is found to saturate at a value close to the Orowan stress. The saturation coincides at large shear resistance with the predominance of Orowan looping to the detriment of shearing. On the other hand, although the precipitate density is quite large, imposing a percolation distance does not seem to alter PH induced by weak precipitates. At high shear resistance, the deviation from PH of full random distributions remains small but becomes significant.

4.2. Effect of thermal activation

At finite temperature, the motion of the dislocation segment inside the precipitate as simulated in DD depends on temperature via the activation energy computed from ASs. Massive DD simulations were performed using different Cr-precipitate sizes and densities. In these simulations, the average dislocation velocity was set to 1.8 m/s, which is in the same order of magnitude of dislocation velocities in mechanical tests. The computed hardening is depicted in Fig. 7 as a function of temperature for different densities (D = 2 nm) and for different precipitate sizes ($C = 4\times10^{24}$ m^{-3}).

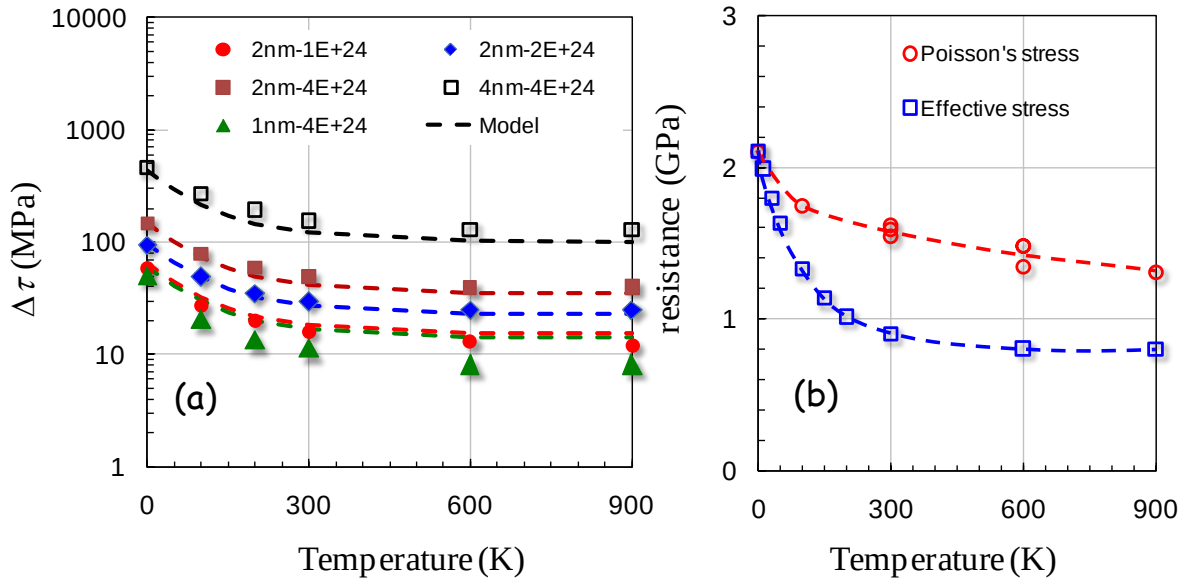

Fig. 7: (a) precipitate hardening induced by Cr precipitates as a function of temperature for different precipitate sizes and densities. Dashed lines are predictions of the model presented in the paper and (b) comparison between the Poisson's stress and the effective stress (see text for more details)

It can be seen that thermal activation strongly decreases PH at low temperature, while no significant effect is found at high temperature, say larger than room temperature. This finding holds for the different precipitate sizes and densities. The ratio between the hardening at zero and at finite temperature is substantially larger than the same ratio computed in ASs. This point is discussed in the next section.

In order to estimate the strain rate sensitivity of the precipitate hardening, we performed two additional series of simulations with different dislocation velocities (0.18 and 18 m/s) for precipitate configuration with D = 2 nm and $C = 4\times10^{24}$ m^{-3}. As expected, results show that PH at 0 K and at 900 K are approximately the same, i.e. independent of the dislocation velocity. However, at intermediate temperature/stress, the sensitivity to the dislocation velocity is significant. PH at 200 K increases from 45 MPa to 85 MPa, when the imposed average velocity of the dislocation is raised from 0.18 to 18 m/s. On the other hand, the activation volume V computed by:

$$V = -kT \times \frac{\Delta \ln(v)}{\Delta \tau}, \qquad (6)$$

is found to decrease monotonously with the stress. Two asymptotic behaviors are observed. *V* goes to zero when the applied stress increases to its quasi-static value, i.e. the PH at 0 K. At low stress, an athermal threshold appears close to 40 MPa, at which the activation volume diverges.

5. Discussion

The analysis of the precipitate strength in terms of resistance stress τ_{obs} presented in this paper offers two advantages: (i) the precipitate resistance expressed as a uniform shearing resistance inside the precipitates allows for a full multi-scale modeling of precipitate hardening with a shear resistance completely characterized from ASs and (ii) the decrease in the pinning stress with the temperature revealed in ASs can be used to deduce the activation energy of the shearing process as a function of the local stress applied on the pinned segments. The agreement between the DD and the AS results with and without thermal activation (Fig. 3b and Fig. 4b) provides direct evidence on the validity of the transition method reported in this work. However, attention must be paid to two important limitations of this approach: (i) in the case of small precipitates (say less than 1.5 nm) the elastic distortion induced by the precipitate coherency can no longer be neglected and (ii) for large precipitates (say larger than 4 nm), precipitates may undergo phase transition induced by shearing, which alters the mechanism of precipitate unpinning.
In DD simulations, precipitates were randomly distributed and all precipitates had the same size. The resulting 3d-arrangement is not the most realistic one [5]. First there is a finite distribution in the precipitate size and, second, solute depletion around precipitates prevent precipitate nucleation in the vicinity of other precipitates. Ronnpagel et coworkers [25,54] proposed a method to avoid these imperfections. In this study we chose the random distribution for the sake of simplicity and safe comparison with available theoretical models. Also no image forces were considered in our work. These forces are expected to be negligible for very small obstacles as pointed out by Shin et al. [55].
In the following we analyze DD results of PH as a function their resistance and simulation temperature.

5.1. Orowan hardening

Our first important result is that predictions of the original BKS model for the Orowan strengthening are not in agreement with DD simulations of interaction with nanometric size precipitates (say less than 20*b*). In their original paper, Bacon et al. [8] reported the presence of a constant ($B = 0.7$) added to the logarithm term in the line tension expression. Since they were interested in precipitates of relatively large sizes, the constant was neglected in the development of their hardening model. When the precipitate size is within few nanometers, this approximation is thus no longer valid. It happens that this constant is close to ln 2. This is why we considered the normalization by $b/2$, instead of b. This modification is equivalent to a decrease in the inner cut-off radius of the dislocation energy (or line tension) from b to $0.5b$, which is rather in agreement with ASs [49,56]. The new expression given in Eq.5 is found to strongly improve the agreement with the DD results. Even using the new normalization, DD predictions of Orowan hardening are found systematically larger than predictions of Eq. 5 (see Fig. 5). Nevertheless, the difference between DD results and the theory does not exceed 16%. Other, more sophisticated models of the Orowan hardening

were reported in the literature [1]. However, their agreement with our results is not better than that obtained with the modified BKS model reported in this paper.

5.2. Effect of the shear resistance on hardening

In this part of the paper, we attempt to rationalize simulation results on the effect of shear resistance on PH, depicted in Fig. 5. We restrict our analysis to the case of simulations showing smooth motion of the dislocation. In order to rationalize the DD results, several theoretical models can be tested [57]. Here, we compare our results with predictions of the two most well-known models of hardening induced by local finite-strength obstacles [3]. In the Friedel model [58,59] designed for week point obstacles, the hardening scales with the 3/2 - power of the obstacle force F. Hardening is given by:

$$\Delta\tau_{Friedel} = \frac{1}{lb\sqrt{2\Gamma}} F^{\frac{3}{2}}, \qquad (7)$$

where Γ is the dislocation line tension, taken equal to $\frac{1}{2}\mu b^2$ in the initial model. Of course, the precipitate size is absent from the model since it was designed for point obstacles. In order to apply this model to our simulations, we consider the absolute force of obstacle to be given by $F = bD\tau_{obs}$. Eq. 7 becomes thus:

$$\Delta\tau_{Friedel} = \sqrt{\frac{D^3}{\mu bl^2}} \tau_{obs}^{\frac{3}{2}} \qquad (8)$$

For strong obstacles of finite size, or interaction range w, we can apply the so-called Mott-Labusch model [60,61,62], where hardening is expressed as:

$$\tau_{Labusch} = \sqrt[3]{\frac{F^4 w}{2\mu b^5 l^4}} \qquad (9)$$

In our case, w is naturally considered equal to the precipitate size D and F is replaced by $bD\tau_{obs}$. Eq. 10 becomes:

$$\tau_{Labusch} = \sqrt[3]{\frac{D^5}{2\mu bl^4}} \tau_{obs}^{\frac{4}{3}} \qquad (10)$$

The concept of the shear resistance, computed from ASs, allows thus for direct and simple application of theoretical models, since the obstacle strength is simply $bD\tau_{obs}$. With this approach no need for the ambiguous and confuse concept of the critical angle.

Predictions of Eqs 8 and 10 are compared with DD results in Fig. 5b. It is easy to notice that the Friedel model systematically overestimates PH, in agreement with results of numerical simulations using constant line tension, reported by Foreman and Makin [7] and by Xu and Picu [24]. On the other hand, the Mott-Labusch model predictions underestimate PH, even at large shear resistance. Nevertheless, the two models seem to provide relatively good upper and lower bounds of hardening induced by shearable obstacles.

The new results reported in this paper concerning penetrable and impenetrable precipitates enable us to develop a new model of PH, presented in the next section.

5.3. New model for precipitation hardening at zero temperature

From Fig. 4a, it is easy to notice that for a periodic row of precipitates of resistance τ_{obs}, the hardening saturates at the Orowan hardening, for resistances larger than a given threshold,

denoted by τ_∞. Below τ_∞, hardening increases linearly with τ_{obs}. For periodic row of shearable precipitates, PH can thus be given by:

$$\Delta\tau_{row} = \frac{\tau_{obs}}{\tau_\infty}\tau_{BKS,row} \qquad (11)$$

$\frac{\tau_{obs}}{\tau_\infty}$ appears thus as an interaction coefficient α_{row} accounting for the precipitate strength. This coefficient is equal in the classical approaches to the normalized obstacle strength $F/2\Gamma$, used in constant line tension simulations. Consider now a random distribution of shearable precipitates. When the dislocation motion is smooth, simulation results depicted in Fig. 6a show that PH is also proportional to the Orowan hardening. In other words, it is possible to write $\Delta\tau = \alpha\,\Delta\tau_{Orowan}$, where α is the interaction coefficient of the precipitates. The question now is how to deduce α from α_{row}. The latter represents the individual obstacle strength, while the former accounts for precipitate strength *and* distribution. For the random distribution, considered in this work, the Friedel statistics, connecting the obstacle strength with the effective spacing of obstacles along dislocation lines, suggest that α is proportional to the 3/2 power of the obstacle force. Within our variables, this leads to the equation: $\alpha = (\alpha_{row})^{3/2}$. If we approximate the Orowan hardening $\Delta\tau_{Orowan}$ by predictions of the modified BKS model given in Eq.5, we finally obtain:

$$\Delta\tau = \begin{cases} \left(\dfrac{\tau_{obs}}{\tau_\infty}\dfrac{\ln 2\underline{\underline{D}}}{\ln 2l}\right)^{3/2} \dfrac{\mu}{2\pi\underline{\underline{l}}}\ln(2l), & \tau_{obs} \le \tau_\infty \\ \left(\dfrac{\ln 2\underline{\underline{D}}}{\ln 2l}\right)^{3/2} \dfrac{\mu}{2\pi\underline{\underline{l}}}\ln(2l), & \tau_{obs} \ge \tau_\infty \end{cases} \qquad (12)$$

In Fig. 8, predictions of Eq. 12, are compared with DD results shown in Fig. 6b with pure random distribution. In order to test the extent of validity of Eq. 12, we perform additional DD simulations of PH with a distribution of 2 nm size and 10^{24} m^{-3} density of precipitate of variable resistance. All simulation results together with predictions of Eq. 12 are depicted in Fig. 8. It can be clearly seen that the agreement with DD results is better than that obtained with the two theoretical models tested previously, especially for week obstacles.

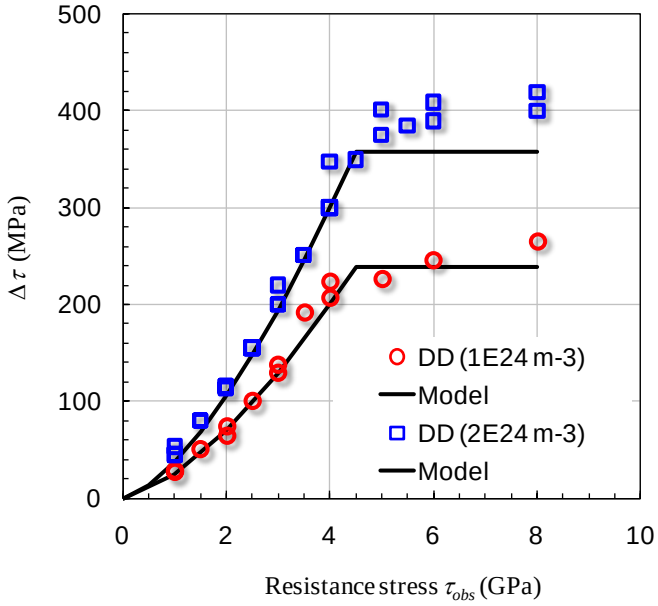

Fig. 8: evolution of precipitation hardening as a function of the shear resistance for 2 nm precipitates and tow different precipitate densities.

In Eq. 12, the geometric properties of precipitates are represented by the free spacing l and size D of the precipitates. The physical nature of the precipitates inducing their pinning force is implicitly accounted for by τ_{obs}. However, the precise value of τ_∞ to be considered is not clear. This variable plays the role of a threshold resistance beyond which PH is constant and equals the Orowan hardening. Its value can in principle be deduced from DD simulations by recording the shear resistance beyond which Orowan looping occurs. For simulations shown in Fig. 4a, the threshold for Orowan looping was found close to 4.5 GPa, while hardening itself saturates at 3.5 GPa. The maximum unpinning stress is thus reached before the bypassing process starts. This feature is still not clearly understood by the author and deserves further investigations.

On the other hand, the best fit for τ_∞ finally used for predictions shown in Fig. 8 was 4.5 GPa, which is larger than the saturation value of hardening induced by the periodic row (Fig. 4a) and lower than the Orowan limit of 4.5 GPa. This feature can be rationalized owing to the precipitate distribution considered here. The average size of the intersection circles between the slip plane and the randomly distributed precipitates is ($\pi D/4$). The effective size of the interaction circle is 79 % lower than the precipitate size. Since the effective strength of precipitates is proportional to their size, the equivalent value for the saturation stress for the random distribution must be increased by a factor of ($4/\pi$). Accordingly, the saturated stress increases form 3.5 GPa (for periodic row) to 4.4 GPa for the random distribution, which is close to the best fit of the parameter τ_∞. The latter is thus not an adjustable parameter, but can be deduced directly from DD simulations.

5.4. Effect of thermal activation

The model shown in the last section does not account for temperature effects, revealed in ASs (see Fig. 7). The following treatment is based on the simple idea that PH at finite temperature

can be deduced also from Eq. 12 providing that τ_{obs} is decreased with temperature to an appropriate value. The local stress on segments pinned by the obstacles τ_{eff} is the true driving force for thermal activation. When the applied stress increases, τ_{eff} increases faster and the yield stress is reached when the activation rate allows the dislocation to move at the imposed velocity.

The following development is based on the Friedel statistics [59] and inspired from Hiratani et al. [63], who expressed the activation energy as a function of the power of the obstacle strength. Consider therefore a steady state motion of a dislocation of of velocity *v* length *L*, much larger than the average obstacle spacing *l*. The average spacing between obstacles pinning the dislocation is $l_f = l/(\cos\theta/2)^{3/2}$, where θ is the critical cusp angle. As it has been shown before, in our case $\cos(\theta/2) = \tau_{eff}/\tau_\infty$. The number of obstacle pinning the dislocation is thus L/l_f. Since the activation energy $\Delta G(\tau_{eff})$ is known from ASs (see Fig. 2b), the number of activated obstacles per unit time is:

$$n = \frac{L}{l}\left(\frac{\tau_{eff}}{\tau_\infty}\right)^{3/2} \omega_o \exp - \frac{\Delta G\left(\tau_{eff}\right)}{kT}. \qquad (13)$$

After each activation event, the dislocation sweeps a surface equal to l^2. The total swept surface is thus nl^2, which corresponds to an average advance of the dislocation of nl^2/L. Since this distance is obtained in a unit time, it corresponds to the average velocity of the dislocation:

$$v = \left(\frac{\tau_{eff}}{\tau_\infty}\right)^{3/2} \omega_o l \exp - \frac{\Delta G\left(\tau_{eff}\right)}{kT}, \qquad (14)$$

It is interesting to note here that Eq. 14 relates the dislocation average velocity at the *mesoscopic* scale to the activation energy defined at the *atomic* scale, the transition parameter τ_{eff} being identified on both simulation scales. Since the dislocation velocity is connected to the strain rate via the Orowan relation, Eq. 14 provides a relation between the strain rate, temperature and the effective stress. The applied stress is not present in Eq. 14 and $\Delta G(\tau_{eff})$ must not be confused with the activation energy at the mesoscopic scale that can, for example, be measured in experimental mechanical tests. Eq. 14 does not represent an Arrhenius-type rate equation. It determines the value of τ_{eff} that must be reached to accommodate the imposed strain rate at the given temperature. τ_{eff} plays the role of an effective resistance at the given temperature and strain rate. Unfortunately, τ_{eff} cannot be deduced analytically because the curve $\Delta G(\tau_{eff})$ is deduced numerically from ASs and depends on the interaction at the atomic level. As far as Cr precipitates in iron are concerned, Eq. 14 can be resolved in τ_{eff} thanks to the function given in Eq. 2. It has been resolved numerically for every simulation temperature. Values of τ_{eff} fulfilling Eq. 14 are plotted in Fig. 7b, together with the Poisson's stress [18,29], representing the effective resistance of the Cr precipitates at finite temperature in AS conditions. Although, conditions in ASs and in DD simulations were comparable in term of the precipitate spacing and dislocation velocity (few m/s), it can be clearly seen that the effective resistance of Cr precipitates decreases faster in DD than in ASs. This is because of the random distribution implying the presence of the 3/2-power term in Eq. 14.

Once the effective resistance determined, the corresponding PH can be easily computed by replacing the absolute resistance of precipitates τ_{obs} by the effective resistance at finite temperature τ_{eff} in Eq. 12. The finial PH can thus be expressed as:

$$\Delta\tau = \left(\frac{\tau_{eff}}{\tau_\infty} \frac{\ln 2\underline{D}}{\ln 2l} \right)^{3/2} \frac{\mu}{2\pi l} \ln(2l) \ , \qquad (15)$$

with all lengths being normalized by the norm of the Burgers vector. Predictions of Eq. 15 are compared with DD results in Fig. 7a. The temperature effect is slightly overestimated for 4 nm precipitates and underestimated for the 1 nm precipitates. The overall agreement is satisfactory since the precipitate configurations cover multiple sizes and densities over a large range of temperature. It is important to note here that Eqs. 14 and 15 necessary for the prediction of hardening do not contain adjustable parameters.

6. Conclusions

From the results reported in this paper, the following conclusions can be drawn.

1) Atomistic simulations can be used to determine the activation energy of precipitate shearing as a function of the effective stress on the pinned segments.
2) Using the concept of shear resistance, the interpretation of atomistic simulation results allows for successful scale transition and full multiscale simulations of precipitation hardening.
3) DD simulations show that Orowan hardening induced by nanometric obstacles is correctly predicted by the Bacon-Kocks-Scattergood model, providing that the inner cut-off radius of the dislocation energy is taken $b/2$ instead of b.
4) DD simulations reveal that hardening induced by shearable obstacles with and without thermal activation is proportional to the Orowan hardening induced by the same precipitate size and arrangement. The proportionality factor is an interaction coefficient, independent of the precipitate size.
5) The interaction coefficient is a simple 3/2-power of the shear resistance.
6) A simple multiscale model is proposed for the prediction of the precipitation hardening at finite temperature as a function of the precipitate size, density and effective shear resistance.
7) Predictions of the model are in agreement with the precipitation hardening computed in DD simulations of different precipitate size and over a large range of temperature.

Acknowledgment

This work is partially supported by the European project FP7 Project PERFORM60. Details on this project can be found on **www.PERFORM60.net**

References

[1] Martin, J. W. Precipitation Hardening Butterworth-Heinemann Ltd, 1998

[2] Argon, A. Strengthening Mechanisms in Crystal Plasticity OUP Oxford, 2007

[3] Queyreau, S.; Monnet, G. and Devincre, B. Orowan strengthening and forest hardening superposition examined by dislocation dynamics simulations. Acta Materialia, 2010, 58, 5586-5595

[4] Lagerpusch, U.; Mohles, V.; Baither, D.; Anczykowski, B. and Nembach, E. Double strengthening of copper by dissolved gold-atoms and by incoherent SiO2-particles: how do the two strengthening contributions superimpose. Acta Materialia, 2000, 48, 3647-3656

[5] Nembach, E. Particle Strengthening of Metals and Alloys Wiley Professional Software, 1997

[6] Caillard, D. and Martin, J. L. Thermally Activated Mechanisms in Crystal Plasticity. Elsevier Science, 2003

[7] Foreman, A. J. E. and Makin, M. J. Dislocation movement through random arrays of obstacles. Philosophical Magazine, 1966, 14, 911-924

[8] Bacon, D. J.; Kocks, U. F. and Scattergood, R. O. The effect of dislocation self-interaction on the orowan stress. Philosophical Magazine, 1973, 28, 1241-1263

[9] Friedel, J. Dislocations Pergamon Press, 1964

[10] Caillard, D. and Martin, J. L. Thermally Activated Mechanisms in Crystal Plasticity. Elsevier Science, 2003

[11] Weeks, R. W.; Pati, S. R.; Ashby, M. F. and Barrand, P. The elastic interaction between a straight dislocation and a bubble or a particle. Acta Metallurgica, 1969, 17, 1403-1410

[12] Mott, N. F. and Nabarro, F. R. N. An attempt to estimate the degree of precipitation hardening, with a simple model. Proceedings of the Physical Society, 1940, 52, 86

[13] Hirsch, P. B. and Kelly, A. Stacking-fault strengthening. Philosophical Magazine, 1965, 12, 881-900

[14] Bacon, D. J.; Osetsky, Y. N. and Rodney, D. J.P. Hirth and L. Kubin (Eds.) Dislocation-“Obstacle Interactions at the Atomic Level. Dislocations in Solids, Elsevier, 2009, Volume 15, 1-90

[15] Ngan, A. H. W.; Zuo, L. and Wo, P. C. Probabilistic nature of the nucleation of dislocations in an applied stress field. Scripta Materialia, 2006, 54, 589-593

[16] Zhu, T.; Li, J.; Samanta, A.; Leach, A. and Gall, K. Temperature and Strain-Rate Dependence of Surface Dislocation Nucleation. Physical Review Letters, 2008, 100, 025502

[17] Rodney, D. Activation enthalpy for kink-pair nucleation on dislocations: Comparison between static and dynamic atomic-scale simulations. Physical Review B, 2007, 76, 144108

[18] Monnet, G. Determination of the activation energy by stochastic analyses of molecular dynamics simulations of dislocation processes. Philosophical Magazine, 2011, 91, 3810-3829

[19] Monnet, G.; Osetsky, Y. and Bacon, D. Mesoscale thermodynamic analysis of atomic-scale dislocation-obstacle interactions simulated by molecular dynamics. Philosophical Magazine, 2010, 90, 1001-1018

[20] Khater, H. A.; Monnet, G.; Terentyev, D. and Serra, A. Dislocation glide in Fe-carbon solid solution: From atomistic to continuum level description. International Journal of Plasticity, 2014, 62, 34-49

[21] Nogaret, T. and Rodney, D. Finite-size effects in dislocation glide through random arrays of obstacles: Line tension simulations. Physical Review B, 2006, 74, 134110

[22] Altintas, S. and Morris Jr, J. W. Computer simulation of dislocation glideâ€”I. Comparison with statistical theories. Acta Metallurgica, 1986, 34, 801-807

[23] Morris Jr, J. W. and Klahn, D. H. Thermally activated dislocation glide through a random array of point obstacles: Computer simulation. Journal of Applied Physics, 1974, 45, 2027-2038

[24] Xu, Z. and Picu, R. C. Thermally activated motion of dislocations in fields of obstacles: The effect of obstacle distribution. Physical Review B, 2007, 76, 094112

[25] Fuchs, A. and Ronnpagel, D. Comparison between simulation calculations and measurements concerning athermal yielding of precipitation hardening of Cu-Co single crystals. Materials Science and Engineering: A, 1993, 164, 340-345

[26] Mohles, V. and Ronnpagel, D. Thermal activation analysis of dislocations in obstacle fields. Computational Materials Science, 1996, 7, 98-102

[27] Mohles, V.; Ronnpagel, D. and Nembach, E. Simulation of dislocation glide in precipitation hardened materials. Computational Materials Science, 1999, 16, 144-150

[28] Mohles, V. Computer simulations of particle strengthening: lattice mismatch strengthening. Materials Science and Engineering: A, 2001, 319-321, 201-205

[29] Monnet G, Plasticity of Crystalline Materials: from Dislocations to Continuum, G. Ionescu, I. and Bouvier, S. (Eds.), ISTE Ltd., 2011, 3-36

[30] Mohles, V.; Ronnpagel, D. and Nembach, E. Simulation of dislocation glide in precipitation hardened materials. Computational Materials Science, 1999, 16, 144-150

[31] Mohles, V. and Nembach, E. The peak- and overaged states of particle strengthened materials: computer simulations. Acta Materialia, 2001, 49, 2405-2417

[32] Osetsky, Y. N.; Bacon, D. J. and Mohles, V. Atomic modelling of strengthening mechanisms due to voids and copper precipitates in iron. Philosophical Magazine, 2003, 83, 3623-3641

[33] Bacon, D. J. and Osetsky, Y. N. Modelling dislocation-obstacle interactions in metals exposed to an irradiation environment. Materials Science and Engineering: A, 2005, 400-401, 353-361

[34] Terentyev, D. A.; Bonny, G. and Malerba, L. Strengthening due to coherent Cr precipitates in Fe-Cr alloys: Atomistic simulations and theoretical models. Acta Materialia, 2008, 56, 3229-3235

[35] Terentyev, D.; Haghighat, S. M. H. and Schaublin, R. Strengthening due to Cr-rich precipitates in Fe-Cr alloys: Effect of temperature and precipitate composition. Journal of Applied Physics, 2010, 107, 061806

[36] Kuksenko, V.; Pareige, C.; Genevois, C.; Cuvilly, F.; Roussel, M. and Pareige, P. Effect of neutron-irradiation on the microstructure of a Fe - 12at.%Cr alloy. Journal of Nuclear Materials, 2011, 415, 61-66

[37] Matijasevic, M. and Almazouzi, A. Effect of Cr on the mechanical properties and microstructure of Fe-Cr model alloys after n-irradiation. Journal of Nuclear Materials, 2008, 377, 147-154

[38] Terentyev, D.; Bonny, G.; Domain, C.; Monnet, G. and Malerba, L. Mechanisms of radiation strengthening in Fe-Cr alloys as revealed by atomistic studies. Journal of Nuclear Materials, 2013, 442, 470-485

[39] Mohles, V. and Ronnpagel, D. Thermal activation analysis of dislocations in obstacle fields. Computational Materials Science, 1996, 7, 98-102

[40] Picu, R. C.; Li, R. and Xu, Z. Strain rate sensitivity of thermally activated dislocation motion across fields of obstacles of different kind. Materials Science and Engineering: A, 2009, 502, 164-171

[41] Kampen, N. G. V. Stochastic Processes in Physics and Chemistry. North Holland, 2007

[42] Devincre, B.; Madec, R.; Monnet, G.; Queyreau, S.; Gatti, R. and Kubin, L. Forest, S.; Ponchet, A. & Thomas, O. (Eds.) Modeling crystal plasticity with dislocation dynamcis simulations : the «MICROMEGAS» code. Mechanics of Nano-Objects, 2011, 81-100

[43] Kubin, L. Dislocations, Mesoscale Simulations and Plastic Flow OUP Oxford, 2013

[44] Scattergood, R. O. and Bacon, D. J. Dislocation shear loops in anisotropic crystals. Physica Status Solidi (a), 1974, 25, 395-404

[45] Scattergood, R. O. and Bacon, D. J. The Orowan mechanism in anisotropic crystals. Philosophical Magazine, 1975, 31, 179-198

[46] Bacon DJ. In: Bilby BA, Miller KJ, Willis JR, editors. Fundamentals of deformation and fracture. C.U.P; 1985. p. 401.

[47] Suzuki, T.; Takeuchi, S. and Yoshinaga, H. Dislocation dynamics and plasticity. Springer-Verlag, 1991

[48] Monnet, G.; Naamane, S. and Devincre, B. Orowan strengthening at low temperatures in bcc materials studied by dislocation dynamics simulations. Acta Materialia, 2011, 59, 451-461

[49] Terentyev, D.; Bacon, D. J. and Osetsky, Y. N. Interaction of an edge dislocation with voids in iron modelled with different interatomic potentials. Journal of Physics: Condensed Matter, 2008, 20, 44500

[50] Monnet, G. Investigation of precipitation hardening by dislocation dynamics simulations. Philosophical Magazine, 2006, 86, 5927-5941

[51] Seeger A., Proc 2nd UN int conf on peaceful uses of atomic energy, vol. 6, Geneva; 1958. p. 250

[52] Xu, Z. & Picu, R. C. Thermally activated motion of dislocations in fields of obstacles: The effect of obstacle distribution. Physical Review B, 2007, 76, 094112

[53] Ostwald, W. Über die vermeintliche Isomerie des roten und gelben Quecksilberoxyds und die Oberflächenspannung fester Körper. Z Phys. Chem, 1900, 34, 495-503

[54] Pretorius, T. and Nembach, E. The effects of the degree of randomness of arrays of shearable particles on the critical resolved shear stress of particle strengthened materials. Acta Materialia, 2004, 52, 3807-3812

[55] Shin, C. S.; Fivel, M. C.; Verdier, M. and Oh, K. H. Dislocation-impenetrable precipitate interaction: a three-dimensional discrete dislocation dynamics analysis. Philosophical Magazine, 2003, 83, 3691-3704

[56] Monnet, G. and Terentyev, D. Structure and mobility of the edge dislocation in BCC iron studied by molecular dynamics. Acta Materialia, 2009, 57, 1416-1426

[57] Patinet, S.; Bonamy, D. and Proville, L. Atomic-scale avalanche along a dislocation in a random alloy. Physical Review B, 2011, 84, 174101

[58] Fleischer, R. L., Solute dislocations and long range pinning of dislocations. Acta Metallurgica, 1961, 9, 1034-1035

[59] Friedel, J. Dislocations Pergamon Press, 1964

[60] Labusch, R. A, Statistical Theory of Solid Solution Hardening. Phys. Stat. Solid. (b), 1970, 41, 659-669

[61] Nabarro, F. R. N., The statistical problem of hardening. Journal of the Less Common Metals, 1972, 28, 257-276

[62] Neuhauser, H. and Schwink, C., Solid Solution Strengthening, Materials Science and Technology, Wiley-VCH Verlag GmbH & Co. KGaA, 2006

[63] Hiratani, M.; Zbib, H. M. & Khaleel, M. A., Modeling of thermally activated dislocation glide and plastic flow through local obstacles. International Journal of Plasticity, 2003, 19, 1271-1296